

Raman spectroscopy of nanocrystalline diamond: An *ab initio* approach

J. Filik, J. N. Harvey, N. L. Allan, and P. W. May*
School of Chemistry, University of Bristol, Bristol BS8 1TS, United Kingdom

J. E. P. Dahl, S. Liu, and R. M. K. Carlson
MolecularDiamond Technologies, ChevronTexaco Technology Ventures, P.O. Box 1627, Richmond, California 94802, USA
 (Received 8 December 2005; revised manuscript received 29 April 2006; published 19 July 2006)

The use of Raman spectroscopy to detect nano-sized diamond crystals is controversial; the origins of peaks at $\sim 1150\text{ cm}^{-1}$ in chemical vapor deposition nanodiamond films and $\sim 500\text{ cm}^{-1}$ in nanodiamond particles, which have both been suggested as evidence for nanophase material, remain uncertain. Many studies have produced evidence showing that the $\sim 1150\text{ cm}^{-1}$ peak is in fact due to polyacetylenelike structures at grain boundaries and interfaces, but little work has been done to confirm the assignment of the $\sim 500\text{ cm}^{-1}$ peak. In this paper we approach the problem from the molecular level, using Hartree-Fock theory to calculate the Raman spectra of diamond hydrocarbons, and observe the variation of the spectra with molecular size. Molecules with T_d symmetry are studied, varying in size from adamantane to $C_{84}H_{64}$, an octahedral 1 nm-sized diamond crystallite. For comparison with nanodiamond thin films, the mass of the terminal hydrogen atoms were artificially increased to 100 amu, approximating the effects of matrix isolation. The calculated spectra are discussed in terms of the signals commonly observed in the Raman spectra of nanocrystalline diamond samples. This study finds no evidence for Raman active vibrations of diamond nanocrystals at either $\sim 1150\text{ cm}^{-1}$ or $\sim 500\text{ cm}^{-1}$, whether hydrogen terminated or confined in a matrix. Further, it appears that the only signals produced by a nanodiamond crystal are the broadened zone-center (1332 cm^{-1}) mode and low frequency ($<100\text{ cm}^{-1}$) deformations/Lamb-type vibrations. This suggests any other peaks observed in the Raman spectra of nanocrystalline diamond are due to defects, surface structures, amorphous material, or any other nondiamond material in the sample, and should not be taken as definitive evidence of nanocrystalline diamond.

DOI: [10.1103/PhysRevB.74.035423](https://doi.org/10.1103/PhysRevB.74.035423)

PACS number(s): 78.30.Ly, 61.46.Hk, 63.22.+m, 81.05.Uw

I. INTRODUCTION

Raman spectroscopy is one of the most commonly used techniques for the analysis of carbon-based materials. It is routinely used as a simple nondestructive method to analyze a wide range of carbon samples, from amorphous to crystalline. The Raman spectra of single crystal diamond consists of a Brillouin zone-center (Γ point) T_{2g} mode at 1332 cm^{-1} , but various other peaks have been observed in the Raman spectra of micro and nanocrystalline diamond thin films.

The most controversial of these is the peak observed at 1150 cm^{-1} in the Raman spectrum of chemical vapor deposited (CVD) nanocrystalline diamond films. For many years it had been proposed that this peak originates from phonon modes with $q \neq 0$, activated by the disorder induced by small grain sizes in nanocrystalline or amorphous diamond.^{1,2} This idea was reinforced by a maximum in the diamond vibrational density of states (at the L point) at a similar wave number ($\sim 1240\text{ cm}^{-1}$). Recently, this theory has been rejected by a number of groups³ for many reasons, including hydrogen isotope studies⁴ and peak dispersion and intensity variation in resonant Raman spectroscopy using multiple excitation wavelengths⁵ (633–244 nm). It has also been suggested that the diamond crystallites for which this peak were observed were not sufficiently small to allow phonons from the L point to be active in the Raman spectrum.⁵ The results from these experiments suggest the mode is more likely due to polyacetylene-type structures located at grain boundaries and interfaces.

This type of problem is not limited to nanodiamond thin films. The Raman spectrum of shock synthesized nanodiamond powders also contains unassigned signals. In this case the mode of interest produces a broad signal around 500 cm^{-1} tentatively assigned as originating from transverse acoustic phonons near the Brillouin zone boundary or an amorphous sp^3 phase.^{2,6}

Generally, any variation in the Raman spectrum of a nanocrystalline phase is described by relaxation of the $q=0$ selection rule, due to uncertainty in the value of the wave vector. This permits the activation of phonons that would not usually be observed in the Raman spectrum of the bulk material. Instead of taking the bulk material and studying the effects of reducing its size, it is often useful to take a molecule or small cluster reflecting the structure of the material and study the effects of enlarging it.

The Raman spectra of single crystal and microcrystalline graphite were first studied by Tuinstra and Koenig in 1970.⁷ They observed a single peak at 1575 cm^{-1} for single crystal graphite which they attributed to the Brillouin zone-center ($q=0$) E_{2g} mode of the infinite crystal. The microcrystalline sample had a second accompanying peak at 1355 cm^{-1} which was ascribed to a Brillouin zone boundary A_{1g} mode, activated by particle size effects.

Recently, large polycyclic aromatic hydrocarbons (PAH—hydrogen terminated, molecularly defined, subunits of the graphite lattice) have been produced and studied as models for nanosized graphitic domains in carbon materials.^{8–11,13} PAH are small enough to study computationally, and have

been used to show that it is possible to relate the vibrational spectra of these large molecules to the nanocrystalline phase.

In 1991 Shen *et al.*¹² used molecular mechanics, semi-empirical self-consistent field (SCF) methods and *ab initio* SCF theory to study small hydrogen-terminated carbon clusters as an approximation to diamond. Their comparison was based on calculated carbon-carbon bond lengths, total energies, and heats of formation of finite carbon clusters of T_d symmetry, up to $C_{35}H_{36}$. Their study produced useful comparisons of the levels of theory available at that time but suffered from the computing power then available and the lack of experimental data on the clusters.

The isolation of higher diamondoids¹⁴ (hydrogen terminated, molecularly defined, subunits of the diamond lattice) permits us to compare the *ab initio* Raman spectra of these carbon clusters with experiment. After selecting an appropriate level of theory, we consider cluster sizes up to a maximum of ~ 1 nm, and compare the calculated Raman spectra with those measured experimentally for nanodiamond films and powders.

II. THEORETICAL METHODS

Calculations were performed using either Hartree-Fock theory or the three-parameter hybrid functionals of Becke and the correlation functional of Lee, Yang, and Parr (B3LYP). A range of basis sets were used, a selection found as standard in the GAUSSIAN03 (Ref. 15) software suite, and also that of Sadlej.^{16,17} Geometries were optimized using the Berny algorithm, and vibrational frequencies were then computed by determining the second derivatives of the energy with respect to the Cartesian nuclear coordinates. Finally Raman intensities were produced by numerical differentiation of dipole derivatives with respect to the electric field. For very large molecules (up to $C_{969}H_{324}$) the vibrational frequencies (but not Raman intensities) were calculated using a molecular mechanics force field. For these calculations we used the AMBER force field also included in the GAUSSIAN03 software suite.

The diamond structure belongs to the space group $Fd\bar{3}m$; its associated point group is O_h . It is not possible to produce a stable diamondoid molecule with this point group. Some symmetry elements of the O_h group, such as the inversion center, only appear in the infinite diamond lattice. To keep the molecular approximation as close to the bulk as possible, we use the highest symmetry that can be achieved for stable diamond hydrocarbons—the T_d point group. This is useful since the diamond zone-center phonon is triply degenerate (T_{2g}) and this degeneracy is conserved when the symmetry is reduced to T_d . Restricting ourselves to T_d symmetry structures also reduces the computational cost, allowing the study of larger molecules. The constraint of T_d symmetry leaves two distinct shapes of diamond hydrocarbons; tetrahedra and octahedra. Examples of these different shapes are [1(2,3)4] pentamantane,¹⁴ a tetrahedral diamond hydrocarbon and [1231241(2)3] decamantane,¹⁴ an octahedral diamond hydrocarbon.

III. SELECTING THE LEVEL OF THEORY

The first step is to compare the vibrational frequencies and Raman intensities produced by different theories and ba-

sis sets with experimentally determined values. Adamantane (C_{10} with T_d symmetry) is ideal for these purposes, being small enough to be computationally inexpensive but large enough to be broadly similar to diamond. To simplify the comparison, we ignore the high frequency CH stretch region and concentrate solely on the lower frequency vibrational modes that involve motion of the carbon atoms. Figure 1 shows the low frequency region of an experimental Raman spectrum of adamantane and a selection of different calculated spectra. The calculation producing frequencies and intensities closest to those in the experimental spectrum is also the most computationally expensive, using B3LYP and the pVTZ basis set of Sadlej, a combination renowned for cost-effective theoretical vibrational spectra.¹⁸ The vibrational frequencies (excluding the CH stretch modes) produced by this method are in error by $\sim 1.3\%$ when multiplied by the recommended scale factor of 0.9726. Sadly it is not possible to use this combination for any molecules larger than adamantane because the computational cost is far too great. To try to model effectively the Raman spectrum of a nanodiamond crystal it is clear that a compromise is needed. Using a lower level of theory and a smaller basis set considerably reduces the accuracy of the calculation, but allows larger molecules to be studied thereby improving the approximation of using a diamond hydrocarbon as a model for nanodiamond.

The other spectra shown in Fig. 1 are calculated with the following methods; (c) B3LYP/6-31G*, (d) HF/6-31G*, (e) HF/3-21G, and (f) HF/STO-3G. The combination used in (c) is generally seen as the best to use for larger molecules and has frequently been applied to adamantane and its derivatives.¹⁹⁻²¹ After multiplying the calculated vibrational frequencies by the recommended scale factors²² there appears to be little difference between the frequencies and intensities produced by the different calculations. Percentage errors vary between 2 to 3% from B3LYP/6-31G* to HF/STO-3G (again the CH stretch modes were not included in the error calculation). Increasing the size of the molecule to the C_{26} hydrocarbon ([1(2,3)4] pentamantane, the largest molecule in this study for which experimental data is available) yields similar results. This molecule is too large for the B3LYP/Sadlej method, but all other methods produce similar results, although the HF/STO-3G calculation is slightly poorer. The above investigation suggests that HF/3-21G is the optimum method to use, permitting the calculation of vibrational frequencies and Raman intensities of very large molecules of this type with acceptable accuracy.

Using this level of theory and working within the T_d symmetry constraint permits the study of a reasonable selection of molecules, shown in Fig. 2. The smallest molecule (a) $C_{10}H_{16}$ is adamantane, the molecule used to select the level of theory. The bottom row contains the tetrahedral molecules, for which an experimental Raman spectrum only exists for (f) $C_{26}H_{32}$ ([1(2,3)4] pentamantane). The top row are the octahedral molecules, for which there are no experimental spectra. All of the carbons in the octahedral group are tertiary or quaternary except for the apexes of the octahedra which are secondary. It is possible to remove these secondary carbon atoms, effectively truncating the molecule,

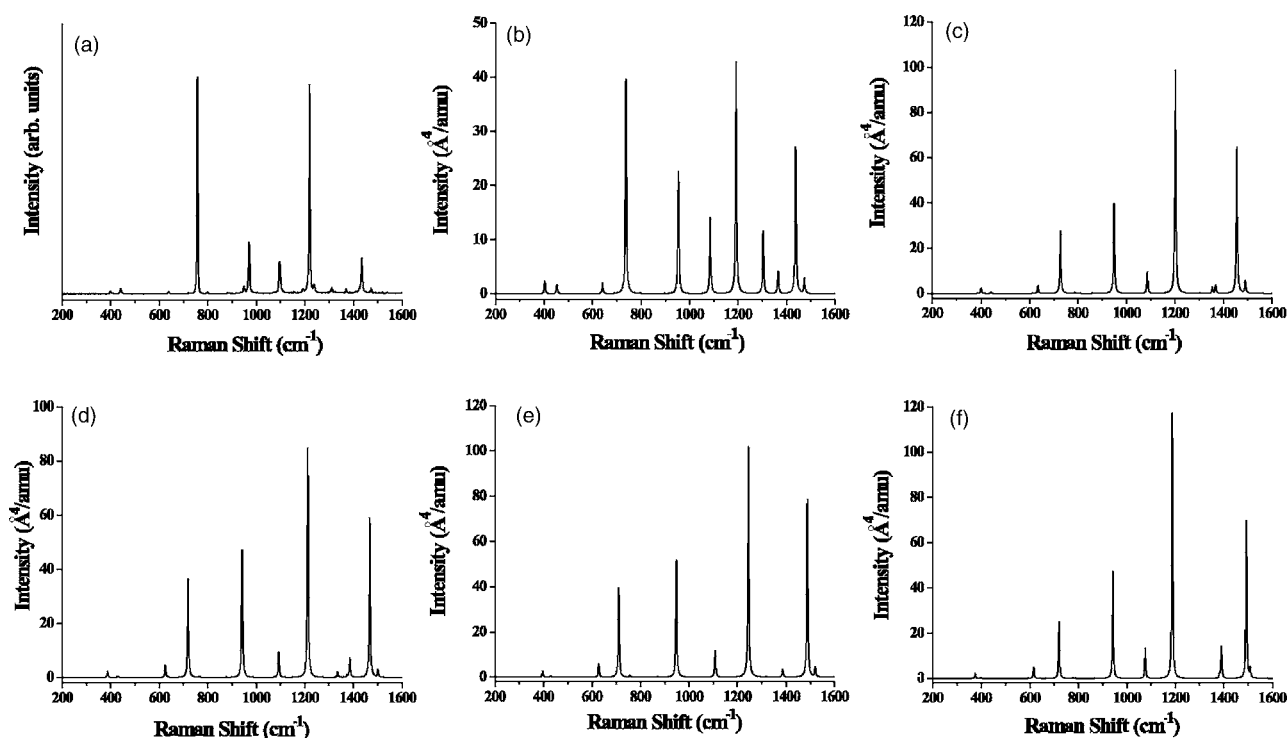


FIG. 1. Raman spectra of adamantane, experimental (Ref. 24) and calculated (with scale factors), (a) experimental, (b) B3LYP/Sadlej (0.9726), (c) B3LYP/6-31G* (0.9603), (d) HF/6-31G* (0.8985), (e) HF/3-21G (0.9056), and (f) HF/STO-3G (0.8165).

producing a cuboctahedral structure. By removing these atoms we are effectively performing a (100) surface reconstruction on the molecule, removing the CH_2 groups and bonding the remaining dangling bonds together. Two possible molecules can be produced in this way. The first [Fig.

2(d)] leaves a single hydrogen atom on each carbon in the bond $[\text{C}(100)2 \times 1:\text{H}]$, while the second [Fig. 2(e)] leaves the carbons π -bonded $[\text{C}(100)2 \times 1]$. To check for any side effects from using only T_d symmetry molecules, the vibrational frequencies and Raman intensities were calculated

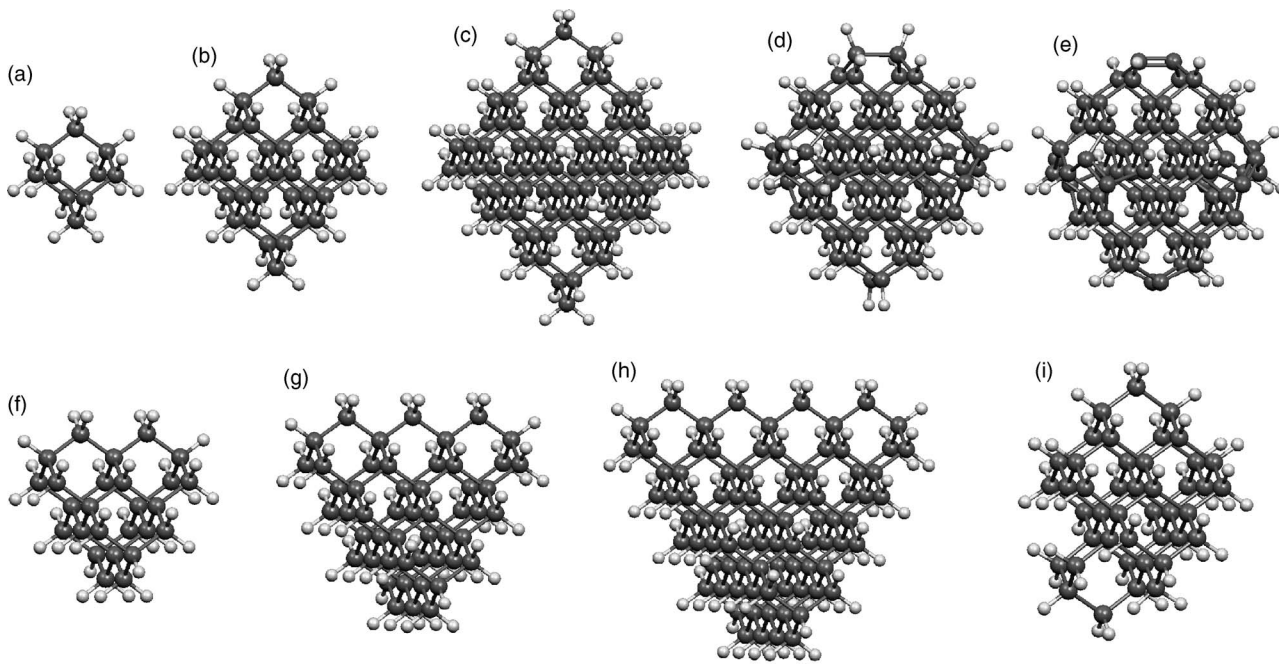


FIG. 2. Octahedral diamond hydrocarbons, (a) $\text{C}_{10}\text{H}_{16}$, (b) $\text{C}_{35}\text{H}_{36}$, (c) $\text{C}_{84}\text{H}_{64}$; (001) reconstructed octahedral diamond hydrocarbons (d) $\text{C}_{78}\text{H}_{52}$, (e) $\text{C}_{78}\text{H}_{40}$; tetrahedral diamond hydrocarbons (f) $\text{C}_{26}\text{H}_{32}$, (g) $\text{C}_{51}\text{H}_{52}$, (h) $\text{C}_{87}\text{H}_{76}$, and (i) the C_1 symmetry diamond hydrocarbon $\text{C}_{43}\text{H}_{44}$.

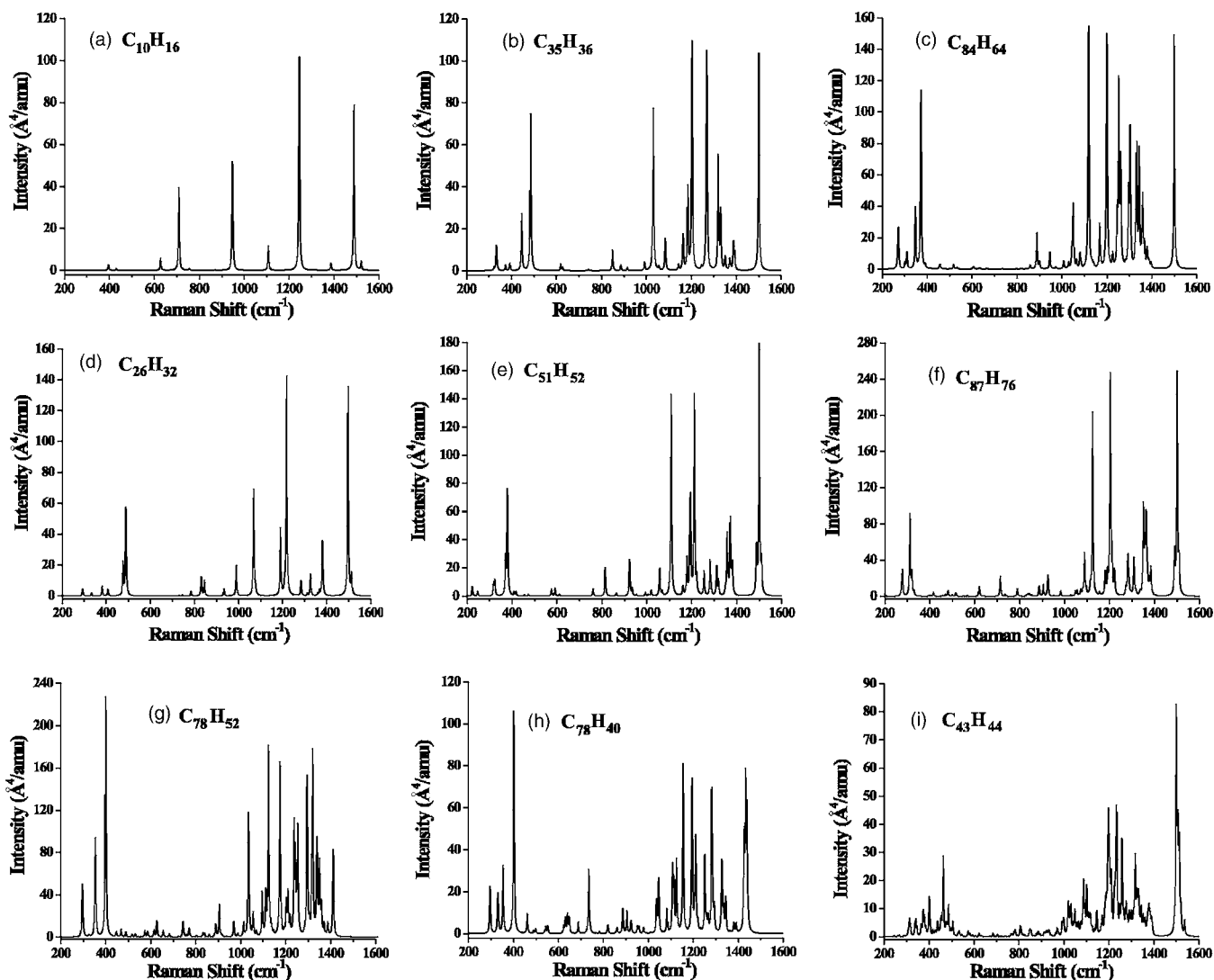


FIG. 3. Calculated Raman spectra for (a) $C_{10}H_{16}$, (b) $C_{35}H_{36}$, (c) $C_{84}H_{64}$, (d) $C_{26}H_{32}$, (e) $C_{51}H_{52}$, (f) $C_{87}H_{76}$, (g) $C_{78}H_{52}$, (h) $C_{78}H_{40}$, and (i) $C_{43}H_{44}$.

for a low symmetry (C_1) diamond hydrocarbon $C_{43}H_{44}$ [Fig. 2(i)].

IV. RESULTS

To study the Raman active vibrational modes in molecules of this type we must first understand the Raman active vibration in diamond. The diamond structure has $Fd\bar{3}m$ symmetry and consists of two interpenetrating face-centered-cubic Bravais lattices, displaced along the body diagonal of the cubic cell by one quarter length of the diagonal. Alternatively, the structure can be considered as a face-centered-cubic lattice with a two atom basis. Due to the small wave vector of the optical photons, the phonons involved in the Raman scattering of crystalline solids have a very small momentum and only the zone-center phonons participate in the first-order Raman scattering. In diamond, the Raman active triply degenerate zone-center optic mode gives rise to the single first-order Raman signal at 1332 cm^{-1} . Using periodic Hartree-Fock (HF) theory, Causà *et al.*²³ obtained a vibra-

tional frequency of 1484 cm^{-1} (44.5 THz). When scaled using the same factors as used for molecular HF theory²² this reduces to 1342 cm^{-1} , close to the experimental value. The nuclear displacements associated with this phonon mode consists of the two carbon atoms in the basis moving in opposite directions, with all unit cells moving in phase. As the size of the crystal is reduced the Raman peak produced by the optical phonon is observed to shift to lower wave number and broaden due to particle size effects.

The calculated Raman spectra of all the molecules studied here are shown in Fig. 3. The peaks have been given a peak width of 5 cm^{-1} , similar to the peak widths observed in our experimental data.²⁴ None of the spectra consist of a single peak at 1332 cm^{-1} so we are clearly some distance away from an infinite diamond lattice. All the spectra (except for that of $C_{10}H_{16}$) can be separated into three parts (excluding the high frequency CH stretch modes); low frequency modes below 500 cm^{-1} , modes between $1000\text{--}1400\text{ cm}^{-1}$, and a collection of modes at $\sim 1500\text{ cm}^{-1}$. The signals at $\sim 1500\text{ cm}^{-1}$ are all due to CH_2 scissor modes and, as shown

in Fig. 1, are considerably weaker in the experimental than the calculated spectrum.

A. The first-order diamond Raman peak—the crystal-molecule transition

Before we consider how the results of our calculations relate to the controversial peaks observed in the Raman spectra of nano-phase diamond particles, we first discuss how these results relate to the bulk diamond 1332 cm^{-1} Raman signal.

Let us briefly consider the experimental Raman spectra produced by diamond in various forms, from infinite crystal through micro/nanocrystalline and finally to amorphous. The bulk crystal produces a single sharp peak at 1332 cm^{-1} , due to the zone-center optical mode. As the crystallite size is reduced to a few hundred nanometers, this peak starts to broaden and shift to a lower frequency due to the relaxation of selection rules. At some point, the sample loses all long-range order and becomes amorphous. The Raman spectrum of amorphous diamond should resemble a broadened phonon density of states of bulk diamond, as seen for silicon and germanium.²⁵ This is rarely observed for diamond due to the tendency of carbon to form sp^2 hybridized structures, and hence the Raman spectra of amorphous carbon is similar to that of disordered graphite. The diamond phonon density of states contains several peaks,²⁶ most notably at $\sim 1260\text{ cm}^{-1}$ and $\sim 500\text{ cm}^{-1}$. It is not too difficult to see how the appearance of peaks at similar frequencies to these in the Raman spectrum of nanocrystalline diamond are assigned as vibrational modes specific to nano-sized diamond crystals.

The final step in the reduction of crystallite size is towards discrete molecules. Unlike an amorphous network, which produces a broad Raman spectrum, molecules possess Raman spectra containing sharp, discrete signals. It would be expected then, that at a certain point, the reduction of the diamond crystallite size would start to produce discrete, molecular-like signals in the Raman spectrum.

The smallest nanodiamond powders that have been studied by Raman spectroscopy contain particles that vary in size between 2–10 nm with an average grain size of 5 nm. For these particles, the bulk diamond 1332 cm^{-1} mode is downshifted by 7 cm^{-1} and broadened to a full width half maximum (FWHM) of 10 cm^{-1} . These values are slightly lower than predicted by phonon confinement models. For a 5 nm diamond crystallite, Yoshikawa *et al.*⁶ predicted a downshift of 13 cm^{-1} and a FWHM of 38 cm^{-1} .

Returning to the spectra calculated in this study, let us consider the variation in the spectra of the octahedral diamond hydrocarbons with increasing cluster size. The structures and calculated spectra of the octahedral diamond hydrocarbons are shown in Figs. 2 and 3(a)–3(c), respectively. The spectrum of the smallest molecule ($\text{C}_{10}\text{H}_{16}$) contains several intense peaks that are reasonably evenly distributed in the range $600\text{--}1600\text{ cm}^{-1}$. In the spectrum calculated for the next largest octahedral molecule ($\text{C}_{35}\text{H}_{36}$), the intense signals have separated into two groups; the breathing mode/cage deformations below 500 cm^{-1} and the CC stretch/CH bend modes in the region $1000\text{--}1500\text{ cm}^{-1}$. Only

a few weak signals are present between 500 and 1000 cm^{-1} . For the largest octahedral molecule studied here ($\text{C}_{84}\text{H}_{64}$), the frequencies of the breathing mode/cage deformations have reduced to below 400 cm^{-1} , increasing the separation between these two groups of intense signals. This separation of these two intense groups of signals is also observed in the spectra of the tetrahedral diamond hydrocarbons. From this we shall assume that as a cluster becomes larger, towards the grain size found in nanodiamond powders, the frequency of these breathing mode/cage deformations reduces further still and hence would appear far from the broadened bulk diamond mode.

The frequencies of the intense CC stretch/CH bend modes remain within a reasonably constant range ($1000\text{--}1500\text{ cm}^{-1}$) as the cluster size increases. The frequency of the zone-center optic diamond mode also lies within this range. The largest molecule studied here is approximately 1 nm in diameter, while nanodiamond particles have a diameter of $\sim 5\text{ nm}$. Yet the calculated spectrum of the $\sim 1\text{ nm}$ diamond hydrocarbon contains sharp discrete lines over a 400 cm^{-1} range and the experimental Raman spectrum of nanodiamond particles contains a single broadened peak. At some grain size the Raman spectrum of a nanodiamond must change from a single broad peak to the discrete lines calculated for these large diamond hydrocarbons, but when does this change from nanocrystal to molecule occur?

First of all there are limitations to the experimental measurements. Experimental spectra are obtained from powdered samples, not isolated particles. The area of the sample analyzed contains a large number of particles, of various different sizes and structures. This large distribution of particles would lead to increased broadening of the bulk diamond peak, which is already broadened by phonon confinement.

Now consider the calculated data. For the $\sim 1\text{ nm}$ molecule, there are so many peaks due to CC stretching/CH bending modes in the $1000\text{--}1500\text{ cm}^{-1}$ region that the previously well-defined peaks are starting to coalesce. From our results on smaller molecules, in larger systems one would expect this region to become a broad unresolvable peak centered around 1250 cm^{-1} , 80 cm^{-1} lower than the bulk diamond Raman signal. This does not fit well with the experimental downshift of 10 cm^{-1} observed for the 5 nm diamond particles. The problem with considering the coalescence of this group of peaks is that the position and width of the broad feature produced is dependent on the relative intensities of the peaks in this $1000\text{--}1500\text{ cm}^{-1}$ region. We know from previous work that the accuracy of the calculated relative intensities of peaks over this region are poor when using a small basis set.

Figure 4(a) shows the experimental Raman spectrum of the largest isolated diamond hydrocarbon, the tetrahedral $\text{C}_{26}\text{H}_{32}$. It is clear that the intensities of the peaks in the $1300\text{--}1400\text{ cm}^{-1}$ region relative to neighboring peaks are severely underestimated using the HF/3-21G combination [Fig. 4(b)]. Increasing the size of the basis set and adding diffuse and polarization functions greatly improves the agreement between the experiment and theoretical spectra in this region [Figs. 4(c) and 4(d)]. Comparing all the different basis set calculations, it appears that the intensity of the CH_2 scissor ($\sim 1500\text{ cm}^{-1}$) and CH wagging ($\sim 1200\text{ cm}^{-1}$)

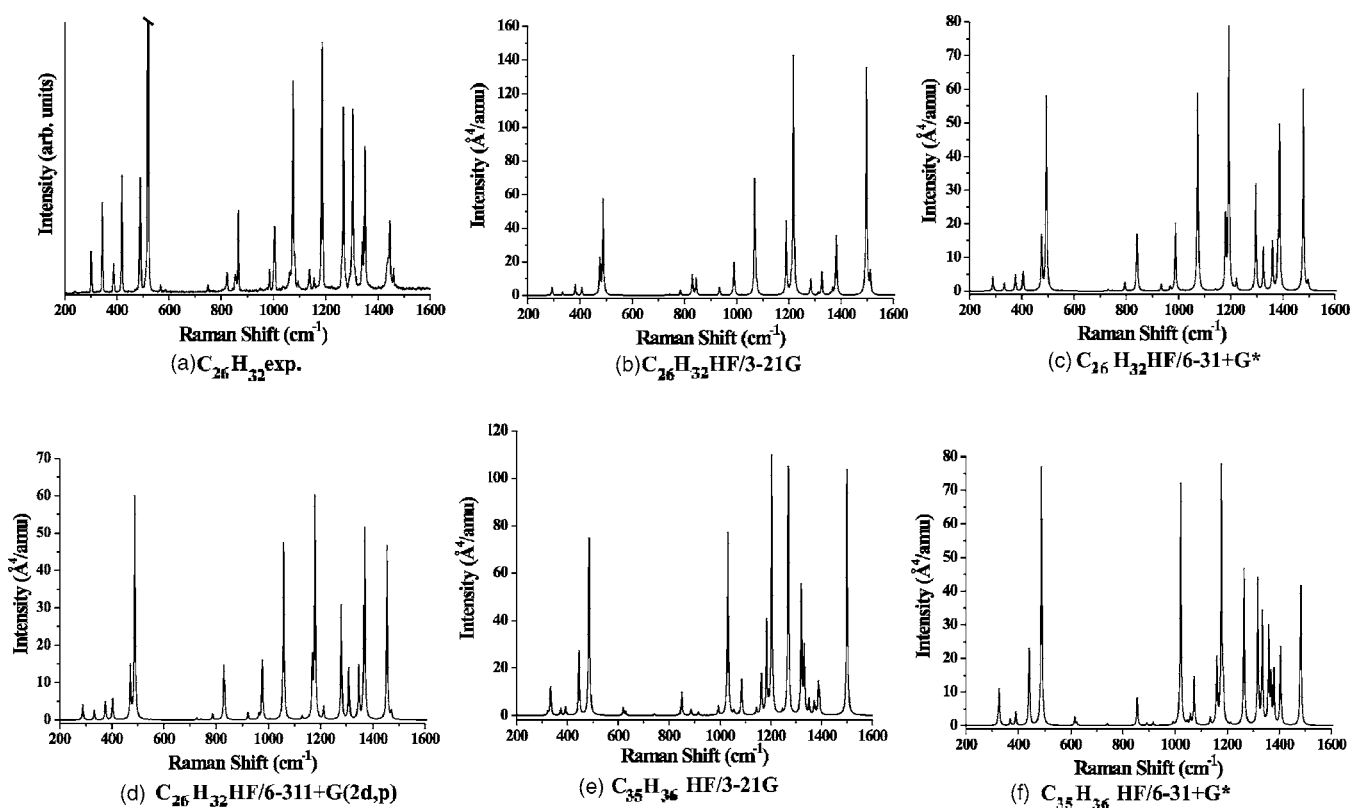


FIG. 4. Raman spectra of diamond hydrocarbons (a) experimental Raman spectrum of $C_{26}H_{32}$ (peak at 518 cm^{-1} cropped for clarity), (Ref. 24) (b), (c), and (d) spectra of $C_{26}H_{32}$, calculated using HF theory and increasingly large basis sets, (e) and (f) spectra of $C_{35}H_{36}$, calculated using HF theory and the 3-21G and 6-31+ G^* basis set, respectively.

modes are strongly overestimated, relative to the $1300\text{--}1400\text{ cm}^{-1}$ region, without the use of both diffuse and polarization functions on carbon atoms. Using HF/6-31+ G^* , the largest diamond hydrocarbon for which we can currently calculate the Raman spectrum for is the octahedral structure $C_{35}H_{36}$.

The HF/3-21G and HF/6-31+ G^* spectra of $C_{35}H_{36}$ are shown in Figs. 4(e) and 4(f), respectively. The same trend observed in the $C_{26}H_{32}$ calculated spectra are also observed here. The $\sim 1200\text{ cm}^{-1}$ CH wagging modes have decreased in intensity and the $1300\text{--}1400\text{ cm}^{-1}$ range now contains many peaks which are beginning to coalesce.

So, if a larger basis set calculation on $C_{35}H_{36}$ shows the beginning of a broadened structure centered around $\sim 1330\text{ cm}^{-1}$, and a reduction in prominence of the intense CH_2 scissors and CH wagging modes, how might this extrapolate to the $\sim 1\text{ nm}$ cluster, $C_{84}H_{64}$? The HF/3-21G calculation on $C_{84}H_{64}$ also showed a cluster of peaks in the range $1300\text{--}1400\text{ cm}^{-1}$ becoming more intense relative to the strong CH wagging and CH_2 scissors modes. We now know that the 3-21G basis set underestimates the intensity of the cluster relative to the wagging/scissors modes. If the 6-31+ G^* basis set could be used for this larger molecule we would expect that the cluster centered around $\sim 1330\text{ cm}^{-1}$ would become even more prominent, becoming a broad signal like that observed in the Raman spectra of nanocrystalline diamond powders.

Complete blurring of the cluster of peaks at $\sim 1330\text{ cm}^{-1}$ into a broad signal has not occurred in any of the spectra of

the large T_d molecules here. However, the spectrum calculated using HF/3-21G for the C_1 symmetry molecule $C_{43}H_{44}$ [Fig. 2(i)] shows a very broad signal over the range $1000\text{--}1400\text{ cm}^{-1}$. The reduction in symmetry splits the degeneracy of the T_2 and E symmetry modes. If, using the HF/6-31+ G^* combination (or better), the Raman spectrum of a large, low symmetry diamond hydrocarbon were calculated, it should start to resemble the broadened optical mode peak seen in the Raman spectrum of nanodiamond particles.

Alternatively, if a sample of identical, perfect, T_d symmetry nanodiamond particles were produced, the broadened optical mode should start to split into well defined peaks due to different surface/bulk mixed vibrations.

B. The $\sim 500\text{ cm}^{-1}$ mode in the Raman spectrum of nanodiamond powders

The most intense peak in the low frequency region of all clusters is produced by the fully symmetric A_1 breathing mode. In the $C_{10}H_{16}$ hydrocarbon this mode appears at 710 cm^{-1} and is calculated to be relatively weaker than observed in the experimental spectrum. From a comparison with experimental data and theory in previous work²⁴ we know that this underestimation continues for $C_{26}H_{32}$, and is therefore likely to be present in all the calculated spectra. The frequency of this breathing mode is strongly dependent on the dimensions of the molecule since it involves a simultaneous stretch of all carbon-carbon bonds in the molecule. This size dependence of the breathing mode frequency is

observed in the calculated data. The frequency of the breathing mode is approximately the same for octahedral and tetrahedral molecules with the same number of carbon-carbon bonds in their edge. For example, $C_{26}H_{32}$ and $C_{35}H_{36}$ both have edge lengths equal to that of five carbon-carbon bonds and a breathing mode frequency of approximately 485 cm^{-1} , $C_{51}H_{52}$ and $C_{84}H_{64}$ have edges composed of seven carbon-carbon bonds and a breathing mode frequency of approximately 375 cm^{-1} . The largest molecule studied here, the tetrahedron $C_{87}H_{76}$, has an edge length of nine carbon-carbon bonds and a corresponding breathing mode frequency of 311 cm^{-1} .

Zhang *et al.*²⁷ have suggested that modes similar to these might be the cause of the broad signal at around 500 cm^{-1} seen in the Raman spectrum of shock synthesized nanodiamond. Their study used density functional theory (B3LYP) and the 6-31G(d) basis set to calculate the vibrational frequencies and Raman intensities of a selection of diamond hydrocarbons, polyaromatic hydrocarbons, and transpolyacetylene chains. To reveal the “characteristic signals” from each of these three types of structure they averaged the calculated Raman spectra of molecules of various sizes. They concluded that only the diamond hydrocarbon average had an intense peak at $\sim 480\text{ cm}^{-1}$, and that this could be used to identify nanocrystalline diamond using Raman spectroscopy.

The results of this study disagree with their assignment. For the diamond hydrocarbons in their study, the modes around 480 cm^{-1} are breathing modes and from what we have seen so far the frequency of these modes is strongly dependent on the size of the molecule. The molecules we are studying are much larger than those studied by Zhang *et al.* but considerably smaller than nanodiamond powders ($\leq 1\text{ nm}$ compared to $\geq 5\text{ nm}$). Even when the size is that of $C_{87}H_{76}$ the frequency of this mode is already far below 500 cm^{-1} .

It is possible to calculate the normal vibrational frequencies (but not Raman intensities) for considerably larger molecules using a molecular mechanics force field instead of an *ab initio* method. Using the AMBER molecular mechanics method included in the Gaussian suite of software we have calculated the vibrational frequencies for octahedral clusters up to $C_{969}H_{324}$ ($\sim 2.8\text{ nm}$ diameter). Again, as the cluster size increases the wave number of the breathing mode decreases (Fig. 5), down to below 200 cm^{-1} for $\sim 2.8\text{ nm}$. It therefore seems unlikely that this type of mode might be responsible for the broad signal at $\sim 500\text{ cm}^{-1}$. It is possible that the breathing mode could be observed in the Raman spectrum of nanodiamond but it would be very close to the Rayleigh line (less than 100 cm^{-1} shift). If this line could be observed, its vibrational frequency should show a strong dependence on the size of the crystallite, producing a fast, nondestructive method of sizing nanodiamond crystals.

Low frequency Raman spectroscopy has been successfully used to determine the size of nanoscale quantum dot structures of various materials^{28–31} by using the size dependent frequency of various acoustic modes. Assignment of the observed modes is generally considered in terms of free vibrations of a homogeneous elastic sphere under stress-free boundary conditions, a theory due to Lamb³² in 1882 which has recently been adopted and modified by many groups.^{33–35}

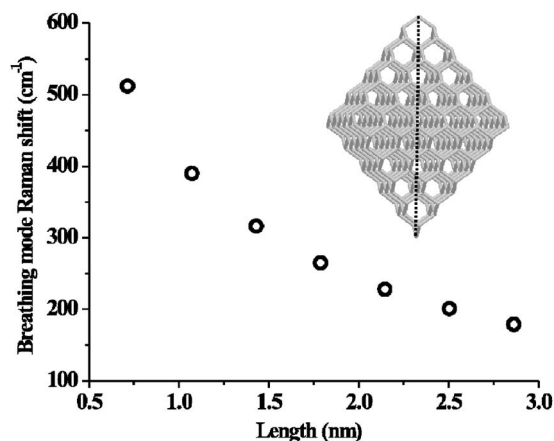


FIG. 5. Variation in the calculated (AMBER) Raman shift of the breathing mode with molecule size. The length plotted was determined from the distance between opposite points of the octahedral structure (see inset).

Lamb’s theory produces two types of vibrational mode, spheroidal and torsional, each with its own set of angular momentum numbers. For example the $l=0$ spheroidal fundamental is similar (but not exactly equivalent to) the breathing mode observed in our calculations. A full study of this theory is beyond the scope of this work, but it would seem that the observation of Lamb modes in the low frequency Raman spectrum would be the easiest way to prove a sample was truly nanocrystalline.

To conclude this section, it appears that there is no simple explanation for the broad $\sim 500\text{ cm}^{-1}$ wave number vibration seen in nanodiamond, but it is unlikely to be due to the full-molecule breathing modes as suggested by Zhang *et al.*²⁷ because of the sharp reduction in the vibrational frequency of this type of mode as the dimensions of the molecules increase. In addition to this, in the previous section we predicted that the other intense peaks observed in the calculated spectra (the $1000\text{--}1400\text{ cm}^{-1}$ region) should coalesce into the broadened optical mode seen in the nanodiamond Raman spectrum. Thus we find no evidence for any strongly Raman active vibrations of nanodiamond, apart from the broadened optical mode and the low frequency breathing/Lamb-type modes. Since the 500 cm^{-1} peak is absent in our perfect diamond molecule model, this peak must be due to imperfections in the nanocrystals or at their surfaces. As part of this work we have briefly studied the (100) defect/surface reconstruction. The (100) 2×1 reconstruction does produce extra signals in the Raman spectra, due to the sp^2 out-of-plane bending modes, but these are at $\sim 750\text{ cm}^{-1}$, far from the $\sim 500\text{ cm}^{-1}$ of the experimental peak. Calculation of the Raman spectra of a selection of common defects/surface reconstructions might well yield a possible assignment of this signal, but it is beyond the scope of this study.

C. Decoupling the hydrogen motion—nanodiamond thin films

The conclusions from the section above can be applied to the Raman spectrum of isolated nanodiamond single crystals (as in nanodiamond powders), but not to thin films of nano-

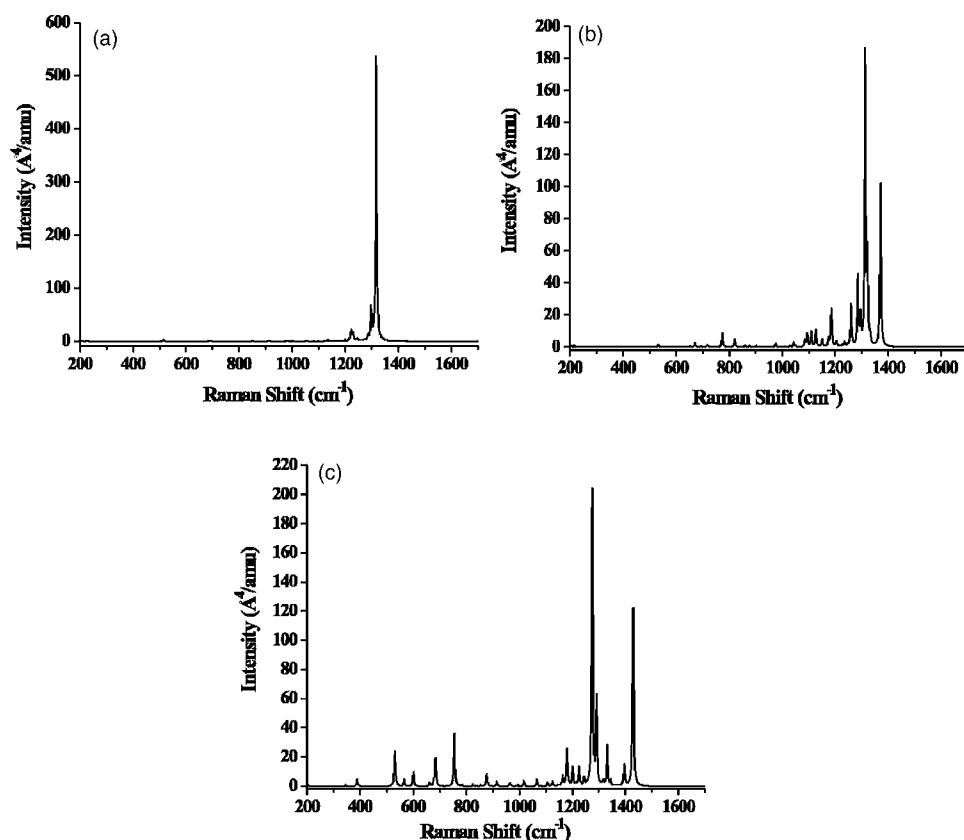


FIG. 6. Calculated Raman spectra for (a) $C_{84}H_{64}$, (b) $C_{78}H_{52}$, (c) $C_{78}H_{40}$, with H mass=100 amu.

diamonds connected by grain boundaries. The approximation of a hydrogenated surface is fair for an isolated crystal, but in a thin film the diamond crystals are covalently bonded to an amorphous carbon matrix.

Previously, Negri *et al.*⁸ have approximated the Raman spectrum of a matrix-confined graphite crystal by taking a hydrogen-terminated PAH molecule and changing the edge-terminating hydrogen mass to 100 amu. This artificial increase in the hydrogen mass separates the frequencies of the bulk stretching modes and surface atom bending modes, removing the strong mode mixing which occurred in the region 1000–1400 cm^{-1} when the mass of H is 1 amu.

In the Raman spectra produced by nanodiamond films the peak assigned as nanophase diamond occurs at $\sim 1150 cm^{-1}$, although the evidence for this being due to polyacetylene structures at surfaces and grain boundaries is very strong.³ Using this H mass=100 amu method of approximating an amorphous carbon network surrounding the diamond crystal, we have calculated the Raman spectra for confined versions of the diamondoid hydrocarbons studied above.

Figure 6 shows the constrained spectra for the octahedral $C_{84}H_{64}$, the $2 \times 1:H$ reconstructed $C_{78}H_{52}$, and the 2×1 reconstructed $C_{78}H_{40}$. The number of signals in the spectra have reduced considerably, especially in the unreconstructed case where there is effectively only one strong signal (1317 cm^{-1}). The nuclear displacements of this mode are very similar to the 1332 cm^{-1} zone-center mode seen in the Raman spectrum of single crystal diamond. It is triply degenerate and is produced by the same carbon-carbon bond stretching motions as described above. This mode is produced by all the diamond hydrocarbons studied here when

constrained, even the small C_{10} structure of adamantane. This suggests that if an adamantane derivative could be synthesized with a full surface termination of a heavy substituent such as bromine, instead of hydrogen, it should have a Raman spectrum very similar to that of diamond. This is confirmed by a HF/3-21G* calculation, although there is a shift in the vibrational frequency of this stretching mode (to 1000 cm^{-1}) caused by strain in the carbon bonds due to the steric repulsion of the large bromine atoms.

The only other peaks in the $C_{84}H_{64}$ spectrum are (i) another stretching mode at 1298 cm^{-1} similar to the diamond zone-center mode but the direction of the stretching motion is opposite on each side of the molecule, and (ii) another weak cluster of CC stretch modes around 1225 cm^{-1} , which is very close to the maximum in the diamond vibrational density of states. These other modes are relatively weak compared to the intense main peak.

The constraining of the two reconstructed diamond hydrocarbons gives us an insight into the effect of imperfections in the grain boundaries of nanodiamond films upon their Raman spectra. The $2 \times 1:H$ reconstruction introduces strain in the molecule and results in significant changes in geometry from that adopted in the diamond structure. This produces a more complex spectrum compared with the unreconstructed molecule, although all the very strong signals still feature vibrations similar to the diamond zone-center mode, just perturbed by the reconstruction.

The 2×1 reconstruction introduces some sp^2 bonds into the structure and hence some new signals into the spectrum. The spectrum of this reconstruction features similar smearing of the diamond zone-center-like vibration as the $2 \times 1:H$, but

there are also signals similar to those seen in the unconfined molecule. The carbon-carbon sp^2 bond stretch is again at $\sim 1420\text{ cm}^{-1}$ and there are also the sp^2 out-of-plane bending modes around 750 cm^{-1} .

The calculated spectrum of confined C_1 symmetry diamond hydrocarbon [Fig. 2(i)] is similar to that of the unreconstructed $C_{84}H_{64}$ (Fig. 6). The only large difference between these two spectra is the broadening of the single sharp peak because of the splitting of the degeneracy of the T_2 mode.

The breathing mode is still present in the spectra for all these constrained structures but there is a considerable decrease in the vibrational frequencies ($C_{84}H_{64}$ reduced to 109 cm^{-1}) and intensities. This does not rule out the use of these breathing modes for sizing nanocrystalline diamond thin films. Much of the low-frequency Raman work mentioned above is performed on quantum dot structures confined in a matrix of various types of glass. The theory produced by Lamb has also been modified to include the effects of a confining material, and they also predict a reduction in frequency dependent on the sound velocities in the matrix material.²⁹

Again, apart from the optical mode and the breathing/Lamb modes, we have seen no evidence for other modes produced by the diamond nanocrystal. This suggests that any extra peaks seen in the Raman spectra of nanocrystalline diamond films are due to defects, or structures at grain boundaries and surfaces.

V. CONCLUSIONS

In this study we have used *ab initio* methods to calculate the Raman spectra of a selection of T_d diamond hydrocarbons up to 1 nm in size. All (H mass=1) spectra consist of three regions, the high wave number CH stretch region, a broad region of strongly mixed CC stretch/CH bend modes between $1000\text{--}1400\text{ cm}^{-1}$, and the low wave number breathing mode/cage deformation region $\leq 500\text{ cm}^{-1}$.

The HF/3-21G level of theory was found to produce (scaled) vibrational frequencies and intensities comparable to higher levels/larger basis sets, although the relative intensities showed marked improvement with the addition of diffuse and polarization functions (6-31+G*).

The model of perfect T_d symmetry clusters is able to explain the changes in the Raman active optical phonon frequencies with particle size. Experimental data are generally obtained from a wide distribution of particle sizes and morphologies. If calculations could be performed on a larger data set featuring lower symmetries, a summation of all the spectra would approach the experimental data. Alternatively, if a powder of nanometer-sized perfect, identical diamond crys-

tals could be produced, its Raman spectrum must resemble those calculated here.

From the strong size dependence of the breathing mode frequency we have shown that these vibrations cannot be the origin of the broad $\sim 500\text{ cm}^{-1}$ signal seen in the Raman spectrum of nanodiamond powders. For a $\sim 1\text{ nm}$ diamond crystallite the breathing mode frequency has already dropped below 400 cm^{-1} . It is possible that this signal may be due to defects or surface reconstructions not featured in this study becoming more prominent as the surface-to-bulk carbon ratio increases. Future work will calculate the Raman spectra of a set of defective diamond particulates to try and determine a likely candidate for the cause of the $\sim 500\text{ cm}^{-1}$ signal. Unfortunately these defects will break the high symmetry of these molecules making these calculations currently too time consuming. The change in breathing mode/cage deformation vibrational frequency observed might be very useful for sizing nanodiamond particles, but the signals would appear closer to the Rayleigh line ($< 100\text{ cm}^{-1}$ shift) than suggested by Zhang *et al.*

By changing the mass of the terminating hydrogen atoms we have shown that the Raman spectrum of a confined diamond crystal will be strongly dependent on the crystal surface termination. This leads us to believe that nanodiamond particles with a hydrogen terminated or reconstructed surface will have a very different Raman spectrum to that of a nanodiamond film where the crystallites are confined within a matrix of amorphous carbon and other crystallites. The Raman spectrum of even small clusters is dominated by a carbon-carbon stretch very similar to that observed in the Raman spectrum of diamond. This suggests that even a section of the diamond lattice as small as a single unit cell, trapped in a matrix should produce a signal close to 1332 cm^{-1} . The problem is whether or not the signal is masked by the signal from the matrix. This is probably the case for all CVD nanodiamond films where the sp^2 grain boundaries have a much higher Raman cross section and are resonantly enhanced.

To conclude, the analysis of the calculated spectra of these diamond hydrocarbons, both confined and unconfined, shows little evidence to suggest any diamond density-of-states-like features in the Raman spectrum of nanocrystalline diamond films and powders. We propose that any such peaks observed are due to defects, surface structures, amorphous material, or any other nondiamond material in the sample, and are not definitive evidence for nanocrystalline diamond within a sample.

ACKNOWLEDGMENTS

The authors wish to thank F. Claeysens for useful discussions and the EPSRC for funding.

- *Electronic address: Paul.May@bristol.ac.uk; URL: <http://www.chm.bris.ac.uk/pt/diamond>
- ¹R. J. Nemanich, J. T. Glass, G. Lucovsky, and R. E. Shroder, *J. Vac. Sci. Technol. A* **6**, 1783 (1988).
- ²S. Praver, K. W. Nugent, D. N. Jamieson, J. O. Orwa, L. A. Bursill, and J. L. Peng, *Chem. Phys. Lett.* **332**, 93 (2000).
- ³A. C. Ferrari and J. Robertson, *Philos. Trans. R. Soc. London, Ser. A* **362**, 2477 (2004).
- ⁴R. Pfeiffer, H. Kuzmany, N. Salk, and B. Gunther, *Appl. Phys. Lett.* **82**, 4149 (2003).
- ⁵A. C. Ferrari and J. Robertson, *Phys. Rev. B* **63**, 121405(R) (2001).
- ⁶M. Yoshikawa, Y. Mori, M. Maegawa, G. Katagiri, H. Ishida, and A. Ishitani, *Appl. Phys. Lett.* **62**, 3114 (1993).
- ⁷F. Tuinstra and J. L. Koenig, *J. Chem. Phys.* **53**, 1126 (1970).
- ⁸F. Negri, C. Castiglioni, M. Tommasini, and G. Zerbi, *J. Phys. Chem. A* **106**, 3306 (2002).
- ⁹M. Rigolio, C. Castiglioni, G. Zerbi, G. Negri, and F. Negri, *J. Mol. Struct.* **563-564**, 79 (2001).
- ¹⁰C. Mapelli, C. Castiglioni, E. Meroni, and G. Zerbi, *J. Mol. Struct.* **480-481**, 615 (1999).
- ¹¹C. Castiglioni, F. Negri, M. Rigolio, and G. Zerbi, *J. Chem. Phys.* **115**, 3769 (2001).
- ¹²M. Z. Shen, H. F. Schaefer, C. X. Liang, J. H. Lii, N. L. Allinger, and P. V. Schleyer, *J. Am. Chem. Soc.* **114**, 497 (1992).
- ¹³C. Castiglioni, C. Mapelli, F. Negri, and G. Zerbi, *J. Chem. Phys.* **114**, 963 (2001).
- ¹⁴J. E. Dahl, S. G. Liu, and R. M. K. Carlson, *Science* **299**, 96 (2003).
- ¹⁵GAUSSIAN 03, Revision A.1, edited by M. J. Frisch, G. W. Trucks, H. B. Schlegel, G. E. Scuseria, M. A. Robb, J. R. Cheeseman, J. A. Montgomery, Jr., T. Vreven, K. N. Kudin, J. C. Burant, J. M. Millam, S. S. Iyengar, J. Tomasi, V. Barone, B. Mennucci, M. Cossi, G. Scalmani, N. Rega, G. A. Petersson, H. Nakatsuji, M. Hada, M. Ehara, K. Toyota, R. Fukuda, J. Hasegawa, M. Ishida, T. Nakajima, Y. Honda, O. Kitao, H. Nakai, M. Klene, X. Li, J. E. Knox, H. P. Hratchian, J. B. Cross, C. Adamo, J. Jaramillo, R. Gomperts, R. E. Stratmann, O. Yazyev, A. J. Austin, R. Cammi, C. Pomelli, J. W. Ochterski, P. Y. Ayala, K. Morokuma, G. A. Voth, P. Salvador, J. J. Dannenberg, V. G. Zakrzewski, S. Dapprich, A. D. Daniels, M. C. Strain, O. Farkas, D. K. Malick, A. D. Rabuck, K. Raghavachari, J. B. Foresman, J. V. Ortiz, Q. Cui, A. G. Baboul, S. Clifford, J. Cioslowski, B. B. Stefanov, G. Liu, A. Liashenko, P. Piskorz, I. Komaromi, R. L. Martin, D. J. Fox, T. Keith, M. A. Al-Laham, C. Y. Peng, A. Nanayakkara, M. Challacombe, P. M. W. Gill, B. Johnson, W. Chen, M. W. Wong, C. Gonzalez, and J. A. Pople (Gaussian, Inc., Pittsburgh, PA, 2003).
- ¹⁶A. J. Sadlej, *Collect. Czech. Chem. Commun.* **53**, 1995 (1988).
- ¹⁷A. J. Sadlej, *Theor. Chim. Acta* **79**, 123 (1991).
- ¹⁸M. D. Halls, J. Velkovski, and H. B. Schlegel, *Theor. Chem. Acc.* **105**, 413 (2001).
- ¹⁹J. O. Jensen, *Spectrochim. Acta, Part A* **60**, 1895 (2004).
- ²⁰L. Bisticic, L. Pejov, and G. Baranovic, *J. Mol. Struct.: THEOCHEM* **594**, 79 (2002).
- ²¹A. Kovacs, and A. Szabo, *J. Mol. Struct.* **519**, 13 (2000).
- ²²A. P. Scott and L. Radom, *J. Phys. Chem.* **100**, 16502 (1996).
- ²³M. Causá, R. Dovesi, and C. Roetti, *Phys. Rev. B* **43**, 11937 (1991).
- ²⁴J. Filik, J. N. Harvey, N. L. Allan, P. W. May, J. E. P. Dahl, S. Liu, and R. M. K. Carlson, *Spectrochim. Acta, Part A* **64**, 681 (2006).
- ²⁵R. Alben, D. Weaire, J. E. Smith, Jr., and M. H. Brodsky, *Phys. Rev. B* **11**, 2271 (1975).
- ²⁶W. Windl, P. Pavone, K. Karch, O. Schutt, D. Strauch, P. Gianozzi, and S. Baroni, *Phys. Rev. B* **48**, 3164 (1993).
- ²⁷D. Zhang and R. Q. Zhang, *J. Phys. Chem. B* **109**, 9006 (2005).
- ²⁸L. Saviot, B. Champagnon, E. Duval, I. A. Kudriavtsev, and A. I. Ekimov, *J. Non-Cryst. Solids* **197**, 238 (1996).
- ²⁹L. Saviot, D. B. Murray, and M. C. MarcodeLucas, *Phys. Rev. B* **69**, 113402 (2004).
- ³⁰M. Fujii, Y. Kanzawa, S. Hayashi, and K. Yamamoto, *Phys. Rev. B* **54**, R8373 (1996).
- ³¹A. Tanaka, S. Onari, and T. Arai, *Phys. Rev. B* **47**, 1237 (1993).
- ³²H. Lamb, *Proc. London Math. Soc.* **13**, 187 (1882).
- ³³W. Cheng, S. F. Ren, and P. Y. Yu, *Phys. Rev. B* **68**, 193309 (2003).
- ³⁴W. Cheng, S. F. Ren, and P. Y. Yu, *Phys. Rev. B* **71**, 174305 (2005).
- ³⁵D. B. Murray and L. Saviot, *Physica E (Amsterdam)* **26**, 417 (2005).